Closed-form expressions on CMUTs with layered anisotropic microplates under residual stress and pressure

Zhikang Li, Libo Zhao*, Yihe Zhao, Jie Li, Tingzhong Xu, Kaiming Hu, Zichen Liu, Ping Yang, Guoxi Luo, Qijing Lin, Shiming Zhang, Martin C. Hartel, Wenming Zhang, and Zhuangde Jiang

***Abstract*—Capacitive micromachined ultrasonic transducers (CMUTs) are promising in the emerging fields of personalized ultrasonic diagnostics, therapy and noninvasive three-dimensional biometric. However, previous theories describing their mechanical behavior rarely consider multi-layer and anisotropic material properties, resulting in limited application and significant analysis errors. This paper proposes closed-form expressions for the static deflection, collapse voltage, and resonant frequency of circular-microplate-based CMUTs, which consider both aforementioned properties as well as the effects of residual stress and hydrostatic pressure. These expressions are established by combining the classical laminated thin plate (CLTP) theory, Galerkin method, a partial expansion approach for electrostatic force, and an energy equivalent method. A parametric study based on finite element method simulations shows that considering the material anisotropy can significantly improve analysis accuracy (~25 times higher than the theories neglecting the material anisotropy). These expressions maintain accuracy across almost the whole working voltage range (up to 96% of collapse voltages) and a wide dimension range (diameter-to-thickness ratios of 20~80 with gap-to-thickness ratios of ~2). Furthermore, their utility in practical applications is well verified using numerical results based on more realistic boundary conditions and experimental results of CMUTs chips. Finally, we demonstrate that the high accuracy of these expressions at thickness-comparable deflection results from the extended applicable deflection range of the CLTP theory when it is used for electrostatically actuated microplates.**

***Index Terms*—CMUTs; Closed-form expressions; Hydrostatic pressure; Laminated anisotropic microplates; Mechanical behavior analysis; Residual stress**

Z. Li is with State Key Laboratory for Manufacturing Systems Engineering, International Joint Laboratory for Micro/Nano Manufacturing and Measurement Technologies, Collaborative Innovation Center of Suzhou Nano Science and Technology, School of Mechanical Engineering, Xi'an Jiaotong Xi'an Jiaotong University, Xi'an, Shaanxi 710049, China, and Department of Bioengineering, California NanoSystems Institute, University of California-Los Angeles, Los Angeles, CA 90095, USA(e-mail:zhikangli@xjtu.edu.cn).

L. Zhao*, Y. Zhao, J. Li, T. Xu, Z. Liu, P. Yang, G. Luo, Q. Lin, and Z. Jiang are with State Key Laboratory for Manufacturing Systems Engineering, International Joint Laboratory for Micro/Nano Manufacturing and Measurement Technologies, Collaborative Innovation Center of Suzhou Nano Science and Technology, School of Mechanical Engineering, Xi'an Jiaotong University, Xi'an, Shaanxi 710049, China (e-mail: libozhao@xjtu.edu.cn, johnzhaoyihe@126.com, xjlijie@stu.xjtu.edu.cn, tingzhongxu@163.com, mhlzc1996@stu.xjtu.edu.cn, pingyang86@xjtu.edu.cn, luoguoxi@xjtu.edu.cn, qjlin2015@xjtu.edu.cn, and zdjiang@xjtu.edu.cn)

K. Hu and W. Zhang are with State Key Laboratory of Mechanical System and Vibration, School of Mechanical Engineering, Shanghai Jiao Tong University, Shanghai 200240, China (e-mail: hukaiming@sjtu.edu.cn and wenmingz@sjtu.edu.cn).

S. Zhang and M. C. Hartel are with Department of Bioengineering, California NanoSystems Institute, University of California-Los Angeles, Los Angeles, CA 90095, USA (e-mail: zhangshimingjlu@gmail.com and martinhartel557@gmail.com).

I. Introduction

CAPACITIVE micromachined ultrasonic transducers (CMUTs) have drawn considerable attention for their widespread applications in personalized ultrasonic diagnostics, three-dimensional (3D) biometrics, gesture recognition and biochemical detection [1-6]. CMUTs are a kind of typical electrostatically actuated microplate-based devices, in which one microplate with its all edges clamped is suspended in parallel over the other fully fixed one. The suspended microplate can produce vibrations under co-action of direct current (DC) and alternating current (AC) voltages to transmit ultrasound waves (ultrasound transmitters), or produce electrical signals under co-action of DC voltage and incident waves to detect ultrasound waves (ultrasound receivers). The mechanical behaviors of CMUTs under those excitations, such as deflection, collapse and resonance, determine their performance. For example, the static deflection determines the electromechanical coupling coefficient, transmitting intensity and receiving sensitivity [7]. The minimum voltage required to force the microplate to collapse (collapse voltage), determines the applicable range of the applied DC voltage and operation modes (non-collapse and collapsed models) [8-11]. Additionally, the resonant frequency is related to the bandwidth and detection resolution, as well as the sensitivity when CMUTs are used as resonators for biochemical detection [12]. These performance-related mechanical parameters essentially depend on both the dimensions of CMUTs and the applied loads. Theoretical study on the relationships of these performance parameters with their dimensions and loads is important because it provides an effective and efficient approach for the design and optimization of CMUTs, significantly reducing the time and cost of device development.

Previously, different theoretical models were proposed to study the nonlinear mechanical behaviors of CMUTs under various loading conditions, including equivalent circuit models

from the point of view of electricity and mechanical models from the point of view of mechanics [13-15]. This study focuses on the mechanical model since it is more advantageous in the analysis of the aforementioned mechanical parameters. For this, Ergun *et al.* [16] considered CMUTs as a spring-mass-capacitor system and proposed a lumped electromechanical model for the mechanical behavior analysis, which neglected the deflection of the microplate and led to an underestimated pull-in voltage. Heller *et al.* [17] and Mura *et al.* [18] employed finite element method (FEM) simulation to obtain relatively accurate results. However, this approach is often time-consuming. Therefore, many researchers were devoted to exploring distributed theoretical models. For instance, the step-by-step linearization method [19, 20], perturbation method of multiple time scales (MTS) [21, 22], displacement iteration pull-in extraction (DIPIE) algorithm [23], shooting method [24], differential quadrature method (DQM) [25] and various reduced-order models [26-31] were developed to study those mechanical parameters. However, the majority of the aforementioned modeling methods were finally evaluated numerically, and the accuracy of the numerical solutions easily fluctuates with the chosen voltage step size [32]. Compared with these numerical methods, closed-form expressions are desirable for the design and optimization of CMUTs because they provide an efficient and reliable approach for mechanical behavior analysis. Towards this end, Liao *et al.* [33] and Chao *et al.* [34] proposed closed-form expressions for pull-in voltages of circular and rectangular microplates, respectively, under residual stresses using reduced-order models. Ahmad and Pratap [35] established a closed-form expression for static deflection analysis using the Galerkin method and the linear term of the Taylor series expansions of electrostatic force. In our previous work [36], closed-form expressions for the static deflection, and pull-in voltage of CMUTs with circular microplates were developed using an improved reduced-order model. However, these closed-form expressions suffered from the following limitations, which inhibited their widespread applications. Firstly, most state-of-the-art models neglected the material anisotropy of the microplate, which could result in significant analysis errors (up to 25% as demonstrated in [37, 38]). Secondly, most studies focused on modeling single-layer microplates, which could not be used for the performance analysis of more general CMUT structures consisting of multilayer microplates. Given these limitations, Zhang *et al.* [39] studied the static deflection and frequency response of CMUTs with multilayer square microplates under different pressures using the Ritz method. However, the material anisotropy of the microplate was not considered in their work. Rahman *et al.* [40] proposed a two-dimensional polynomial function to model the deflection shape of CMUTs with square multilayer microplates. However, their work did not study the effect of the material anisotropy and other performance parameters such as pull-in voltage and resonant frequency. Therefore, to enable more general and accurate analyses of the performance parameters of CMUTs, more efforts are required to establish theoretical models and closed-form expressions which can simultaneously consider the properties of the multilayer and material anisotropy.

Herein, we propose a general reduced-order model, which considers both multilayer and anisotropic material properties, for CMUTs with circular microplates subjected to residual stress and pressure. In this model, the classical laminated thin plate (CLTP) theory, the Galerkin method, a partial expansion approach to approximate the electrostatic force and an energy equivalent method are used to establish closed-form expressions for the pull-in voltage, static deflection and resonant frequency of CMUTs. These closed-form expressions are well validated using a parametric study based on FEM simulations and experimental results of CMUTs chips with multilayer anisotropic microplates. The results demonstrate the high accuracy of our closed-form expressions with the material anisotropy considered ((7~25 times higher than the theories without the material anisotropy considered), as well as their widespread applicability across a wide range of bias voltage (0~96% of collapse voltage) and device dimension sizes (diameter-to-thickness ratios of 20~80). We further discuss the underlying reason for the high analysis accuracy of our closed-form expressions.

II. PROBLEM FORMATION

The schematic of a typical CMUT cell with a circular anisotropic microplate composed of *n* layers is shown in Fig. 1.

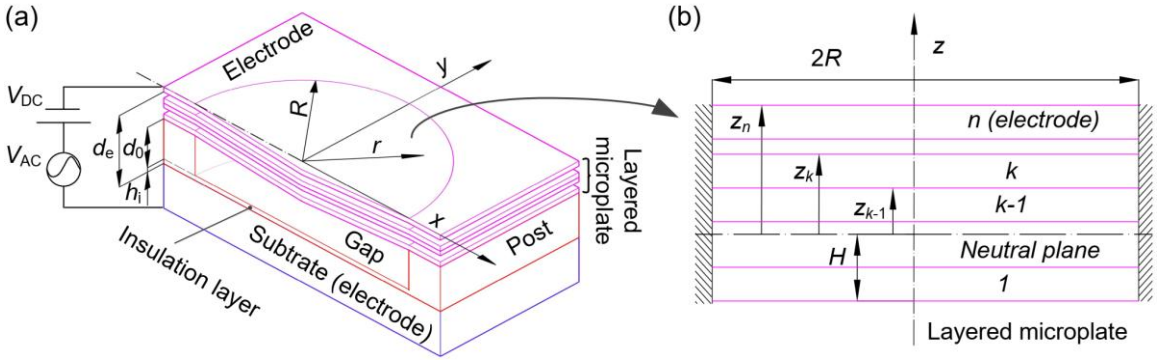

Fig.1. Schematic illustration of a CMUT cell with a layered circular anisotropic microplate; (a) typical structure of CMUTs with multilayer anisotropic microplate, where the substrate works as the bottom electrode; the *n*th layer of the multilayer microplate works as the top electrode, the gap (cavity) shape is circular, the vibrating area of the microplate over the cavity is circular and referred to as "circular microplate"; (b) the enlarged schematic of the layered circular vibrating microplate composed of *n* layers with their edges fully clamped.

The whole microplate as well as each layer is assumed to be thin plates with the same radius of R [41]. The edge of the layered microplate is assumed to be fully clamped. The gap and insulation layer have the thickness of d_0 and h_i, respectively, resulting in an equivalent electrode distance of d_e between the top and bottom electrodes. The layered microplate vibrates under applied DC bias and AC voltages, implementing the operation of CMUTs. The CLTP theory is used to analyze the mechanical behaviors of the CMUTs under electrostatic force and the concerned loads such as residual stress and hydrostatic pressure. In this theory, the bonding between two adjacent layers is assumed to be perfect without any shear deformation, and the transverse shear strains and the strain in the direction normal to the neutral plane are neglected [42]. Additionally, the material of each layer of the microplate is assumed to be orthotropic because the most-often used anisotropic material for CMUTs, silicon, is orthotropic [43]. As such, the vibration governing equation of the layered circular anisotropic microplates of CMUTs under electrostatic force, residual stress and pressure can be written as:

$$\begin{aligned} &D_{11}\frac{\partial^4 w(x,y,t)}{\partial x^4}+2(D_{12}+2D_{66})\frac{\partial^4 w(x,y,t)}{\partial x^2\partial y^2}\\ &+D_{22}\frac{\partial^4 w(x,y,t)}{\partial x^4}+\rho_e h\frac{\partial^2 w(x,y,t)}{\partial t^2}\\ &=P+F_e+N_x\frac{\partial^2 w(x,y,t)}{\partial x^2}+N_y\frac{\partial^2 w(x,y,t)}{\partial y^2} \end{aligned} \tag{1}$$

where P is the hydrostatic pressure; F_e represents the electrostatic force per unit area, given as:

$$F_e=\frac{\varepsilon_0 V^2}{2[d_e-w(x,y,t)]^2} \tag{2}$$

where ε_0 is the permittivity of the gap, and V is the voltage applied to the layered microplate which can be written as:

$$V(t)=V_{bias}+V_{AC}(t) \tag{3}$$

where V_{bias} and $V_{AC}(t)$ represent the applied DC and AC voltages, respectively; correspondingly, the deflection of the layered microplate, $w(x, y, t)$, can be written as:

$$w(x,y,t)=w_{bias}+w_{AC}(x,y,t) \tag{4}$$

where w_{bias} represents the static deflection under V_{bias} and $w_{AC}(x, y, t)$ represents the small vibration around the static deflection; N_x and N_y represent the residual stress of the whole layered microplate in the x and y directions, respectively, which can be obtained by integrating the residual stress over the n layers as:

$$\begin{aligned} N_x&=\sum_{k=1}^{n}\int_{z_{k-1}}^{z_k}\sigma_x^k dz,\\ N_y&=\sum_{k=1}^{n}\int_{z_{k-1}}^{z_k}\sigma_y^k dz \end{aligned} \tag{5}$$

where σ_x^k and σ_y^k represents the residual stress in x and y direction of the kth layer; D_{11}, D_{12}, D_{22} and D_{66} are the equivalent stiffness of the layered microplate (given by (A1)-(A5) in Appendix A), and ρ_e and h are the equivalent density and thickness, respectively (given by (A7)-(A8) in Appendix A).

Using the transformation relations between the polar coordinate system and the Cartesian coordinate system reported in [44], (1) can be further transformed into the polar coordinate system to simplify the mechanical behavior analysis of circular layered anisotropic microplates. Herein, the deflection is assumed to be symmetric because of the symmetry of the circular microplate and the applied loadings. Additionally, the residual stresses in x and y directions are assumed to be uniform and equal to each other, which is a valid assumption for thin plates [38]. As a result, (1) can be rewritten as:

$$\begin{aligned} D'(\frac{\partial^4 w}{\partial r^4}+\frac{2}{r}\frac{\partial^3 w}{\partial r^3}-\frac{1}{r^2}\frac{\partial^2 w}{\partial r^2}+\frac{1}{r^3}\frac{\partial w}{\partial r})+\rho_e h\frac{\partial^2 w}{\partial t^2}\\ =P+F_e+N(\frac{\partial^2 w}{\partial r^2}+\frac{1}{r}\frac{\partial w}{\partial r}) \end{aligned} \tag{6}$$

where D' is given as:

$$D'=\frac{3D_x+2D_k+3D_y}{8} \tag{7}$$

and D_x, D_k, D_y and N are given by:

$$\begin{aligned} &D_x=D_{11},\quad D_y=D_{22},\\ &D_k=D_{12}+2D_{66},\\ &N=N_x=N_y \end{aligned} \tag{8}$$

As the edges of the circular layered anisotropic microplate are clamped, the deflection or vibration function for (6) should satisfy the following boundary conditions:

$$w(R,t)=0 \text{ and } \frac{\mathrm{d}w(r,t)}{\mathrm{d}r}=0 \text{ at } r=R \tag{9}$$

III. Static Behavior Analysis

To obtain closed-form expressions for the deflection and collapse voltage of CMUTs with layered circular anisotropic microplates under DC bias voltage, residual stress and hydrostatic pressure, we used the Galerkin method to establish a reduced-order model for (6). Towards this end, the static deflection function which satisfies the boundary conditions given in (9) is chosen as:

$$w_{bias}(r)=\sum_{m=1}^{M}\eta_m\phi_m(r) \tag{10}$$

where η_m is the coefficient to be determined, and M is the maximum number of the shape functions, $\phi_m(r)$, which is given as:

$$\phi_m=\left[1-(\frac{r}{R})^2\right]^{m+1},\ m=1,2,3\cdots M. \tag{11}$$

Additionally, a partial expansion method developed previously is used to approximate the electrostatic force [36]. Using this method, (2) can be approximated in the polar coordinate system by:

$$F_e(w_{bias}) = \frac{\varepsilon_0 V_{bias}^2}{2d_e(d_e - w_{bias})}(1 + \frac{w_{bias}}{d_e} + \frac{w_{bias}^2}{d_e^2} + \frac{w_{bias}^3}{d_e^3} + \cdots) \quad (12)$$

As such, by setting the time-related terms in (6) to be zero, substituting (10) into the resultant equation, multiplying both sides with $[d_e\text{-}w_{bias}(r)]$ and $\phi_k(r)$, and integrating the resultant equation, a reduced-order model is established as:

$$\begin{aligned} & d_e\int_0^R D'\nabla^4 w_{bias}\times\phi_k \mathrm{d}r - \sum_{m=1}^{M}\eta_m\int_0^R D'\nabla^4 w_{bias}\times\phi_k\phi_m \mathrm{d}r \\ & = \frac{\varepsilon_0 V_{bias}^2}{2d_e}\left(\int_0^R \phi_k \mathrm{d}r + \frac{1}{d_e}\sum_{m=1}^{M}\eta_m\int_0^R \phi_k\phi_m \mathrm{d}r\right. \\ & \left. + \frac{1}{d_e^2}\sum_{m,i=1}^{M}\eta_m\eta_i\int_0^R \phi_k\phi_m\phi_i \mathrm{d}r + \frac{1}{d_e^3}\sum_{m,i,j=1}^{M}\eta_m\eta_i\eta_j\int_0^R \phi_k\phi_m\phi_i\phi_j \mathrm{d}r\cdots\right) \\ & + P\left(d_e\int_0^R \phi_k \mathrm{d}r - \sum_{m=1}^{N}\eta_m\int_0^R \phi_k\phi_m \mathrm{d}r\right) \\ & + N[d_e\int_0^R \nabla^2 w_{bias}\times\phi_k \mathrm{d}r - \sum_{m=1}^{M}\eta_m\int_0^R \nabla^2 w_{bias}\times\phi_k\phi_m \mathrm{d}r] \\ & \qquad \text{for } k = 1,2,3,\cdots M. \end{aligned} \quad (13)$$

where $\nabla^4 w_{bias}$ and $\nabla^2 w_{bias}$ are given as:

$$\nabla^4 w_{bias} = \left(\frac{\mathrm{d}^4 w_{bias}}{\mathrm{d}r^4} + \frac{2}{r}\frac{\mathrm{d}^3 w_{bias}}{\mathrm{d}r^3} - \frac{1}{r^2}\frac{\mathrm{d}^2 w_{bias}}{\mathrm{d}r^2} + \frac{1}{r^3}\frac{\mathrm{d}w_{bias}}{\mathrm{d}r}\right) \quad (14)$$

$$\nabla^2 w_{bias} = \frac{\mathrm{d}^2 w_{bias}}{\mathrm{d}r^2} + \frac{1}{r}\frac{\mathrm{d}w_{bias}}{\mathrm{d}r} \quad (15)$$

Using the fundamental deflection function and the first-order expansion of the electrostatic force, a closed-form expression for CMUTs with circular layered anisotropic microplates under the aforementioned loads can be derived from (13) as:

$$\begin{aligned} w_{bias} = {} & \frac{(1\text{-}r^2/R^2)^2}{32[8D'+0.818NR^2]}\left\{3d_e(56D'+5NR^2)+2PR^4\right. \\ & \left. -2QR^4 - \sqrt{\begin{matrix}[3d(56D'+5NR^2)+2PR^4-2QR^4]^2 \\ -168d_eR^4(P+Q)(8D'+0.818NR^2)\end{matrix}}\right\} \end{aligned} \quad (16)$$

where Q is given as:

$$Q = \varepsilon_0 V_{bias}^2/(2d_e^2) \quad (17)$$

From (16), we can further derive a closed-form expression for collapse voltage by taking advantage of the condition that the corresponding static deflection reaches its maximum value at collapse position. Setting the fifth term in (16) to be zero, the collapse voltage of CMUTs under residual stress and hydrostatic pressure can be obtained as:

$$\begin{aligned} V_{pi} = {} & \frac{d_e}{\sqrt{\varepsilon_0}R^2}\left\{504d_eD'+49.364d_eNR^2+2PR^4\right. \\ & \left. -\sqrt{\begin{matrix}168d_e(8D'+0.818NR^2)(168d_eD' \\ +16.091d_eNR^2+2PR^4)\end{matrix}}\right\}^{\frac{1}{2}} \end{aligned} \quad (18)$$

IV. Natural Frequency for Small-Amplitude Vibration of CMUTs

In the last section, closed-form expressions for static deflection and pull-in voltage were established. Herein, we further studied the small-amplitude vibration of CMUTs under residual stress and hydrostatic pressure, particularly, the first-order natural frequency. For this purpose, we first derived the eigenvalue equation of CMUTs with layered circular anisotropic microplate under electrostatic force, residual stress and hydrostatic pressure. By rewriting (4) into the one in the polar coordinate system, substituting the resultant function into (6), then eliminating the static deflection governing terms in both sides of the resultant equation, expanding w_{AC}-related electrostatic force terms at the static deflection, w_{bias}, and neglecting those higher-order terms (V_{DC}>>V_{AC} for small-amplitude vibration [8, 9, 45]), an approximate eigenvalue equation for CMUTs under the aforementioned loads can be obtained as:

$$\begin{aligned} & D'\nabla^4 w_{AC}(r,t) + \rho_e h\frac{\partial^2 w_{AC}(r,t)}{\partial t^2} \\ & \qquad = \frac{\varepsilon_0 V_{bias}^2 w_{AC}(r,t)}{(d_e - w_{bias})^3} + N\nabla^2 w_{AC}(r,t) \end{aligned} \quad (19)$$

The vibration function, $w_{AC}(r, t)$, in (19) can be written into the product of a shape-related mode function and a time-related harmonic function as:

$$w_{AC}(r,t) = c\eta(\mathrm{r})\sin(\omega\,\mathrm{t}) \quad (20)$$

where $\eta(r)$ and ω are the mode function and angular frequency, respectively. By substituting (20) into (19), the eigenvalue equation can be further simplified as:

$$D'\nabla^4\eta(r) - \omega^2\rho_e h\eta(r) = \frac{\varepsilon_0 V_{bias}^2\eta(r)}{(d_e - w_{bais})^3} + N\nabla^2\eta(r) \quad (21)$$

To solve (21) analytically, we used an energy equivalent method to transform the distributed-parameter-based deflection, $w_{bias}(V_{bias}, r)$, into an equivalent lumped deflection, $w_{eff}(V_{bias})$ [46].This method assumes that the works done by the w_{bias}- and w_{eff}-related electrostatic forces are the same within the same deflection, which can be expressed as:

$$\begin{aligned} & \int_0^R\int_0^{2\pi}\frac{\varepsilon_0 V_{bias}^2\eta(r)}{(d_e - w_{bias})^3}\eta(r)r\,dr\,d\theta \\ & = \int_0^R\int_0^{2\pi}\frac{\varepsilon_0 V_{bias}^2\eta(r)}{(d_e - w_{eff})^3}\eta(r)r\,dr\,d\theta \end{aligned} \quad (22)$$

By evaluating (22), the equivalent lumped deflection, w_{eff}, can be obtained as:

$$w_{eff} = d_e - \left\{\begin{matrix}R^{10}/\left(\frac{5AR^6 - 3d_eR^2}{160A^2(d_e - AR^4)}\right. \\ \left. + \frac{3}{320\sqrt{d_eA^5}}\ln\frac{\sqrt{d_e}+\sqrt{A}R^2}{\sqrt{d_e}-\sqrt{A}R^2}\right)\end{matrix}\right\}^{1/3} \quad (23)$$

where A is set as:

$$A=\frac{1}{32R^4\left(8D'+0.818NR^2\right)}\left\{3d_e(56D'+5NR^2)+2PR^4 -2QR^4-\sqrt{\begin{matrix}[3d_e(56D'+5NR^2)+2PR^4-2QR^4]^2\\ -168dR^4(P+Q)(8D'+0.818NR^2)\end{matrix}}\right\} \tag{24}$$

Substituting w_{bias} in (21) with w_{eff}, the resultant equation can be rewritten as:

$$(\nabla^2+\beta^2)(\nabla^2-\alpha^2)\eta(r)=0 \tag{25}$$

where

$$\alpha^2=\frac{1}{2}\sqrt{\left(\frac{N}{D'}\right)^2+4\left(\frac{\omega^2\rho_e h}{D'}+\frac{\varepsilon_0 V_{\text{bias}}^2}{D'(d_e-w_{\text{eff}})^3}\right)}+\frac{N}{2D'}$$
$$\beta^2=\frac{1}{2}\sqrt{\left(\frac{N}{D'}\right)^2+4\left(\frac{\omega^2\rho_e h}{D'}+\frac{\varepsilon_0 V_{\text{bias}}^2}{D'(d_e-w_{\text{eff}})^3}\right)}-\frac{N}{2D'} \tag{26}$$

As the axisymmetrical vibration of the circular microplate is concerned (without diametrical lines), the corresponding modal function can be expressed as [47]:

$$\eta(r)=C_1J_0(\alpha r)+C_2I_0(\beta r) \tag{27}$$

where J_0 and I_0 are the Bessel function of the first kind of zero order and the modified Bessel function of the first kind of zero order, respectively. The expression (27) can be evaluated using boundary conditions given in (9). Substituting (27) into (9), we can obtain:

$$\begin{matrix}C_1J_0(\alpha R)+C_2I_0(\beta R)=0\\ C_2\beta I_1(\beta R)-C_1\alpha J_1(\alpha R)=0\end{matrix} \tag{28}$$

To obtain non-zero solutions to the coefficients C_1 and C_2, the determinant of (28) should be equal to zero, that is:

$$\det\begin{vmatrix}J_0(\alpha R) & I_0(\beta R)\\ -\alpha R J_1(\alpha R) & \beta R I_1(\beta R)\end{vmatrix}=0 \tag{29}$$

Equation (29) determines the natural frequency of CMUTs with layered circular anisotropic microplates under electrosatic force, residual stress and pressure. It can be solved by combining the underlying relationship between α and β, that is, $(\alpha R)^2-(\beta R)^2=NR^2/D'$. As such, the resonant frequency can be obtained as:

$$f=\frac{\beta^2}{2\pi}\sqrt{\frac{D'}{\rho_e h}}\sqrt{1+\frac{N}{\beta^2D'}-\frac{10\varepsilon_0V_{\text{bias}}^2B}{\beta^4D'R^{10}}} \tag{30}$$

where

$$B=\frac{5AR^6-3d_eR^2}{16A^2(d_e-AR^4)}+\frac{3}{32\sqrt{d_eA^5}}\ln\frac{\sqrt{d_e}+\sqrt{A}R^2}{\sqrt{d_e}-\sqrt{A}R^2} \tag{31}$$

For the vibrating microplate without residual stress, the determinant given in (29) can be transformed into the common one as given in [48] because $\alpha R=\beta R$. The well-known value of βR, 3.196, for the first-order frequency can be directly used.

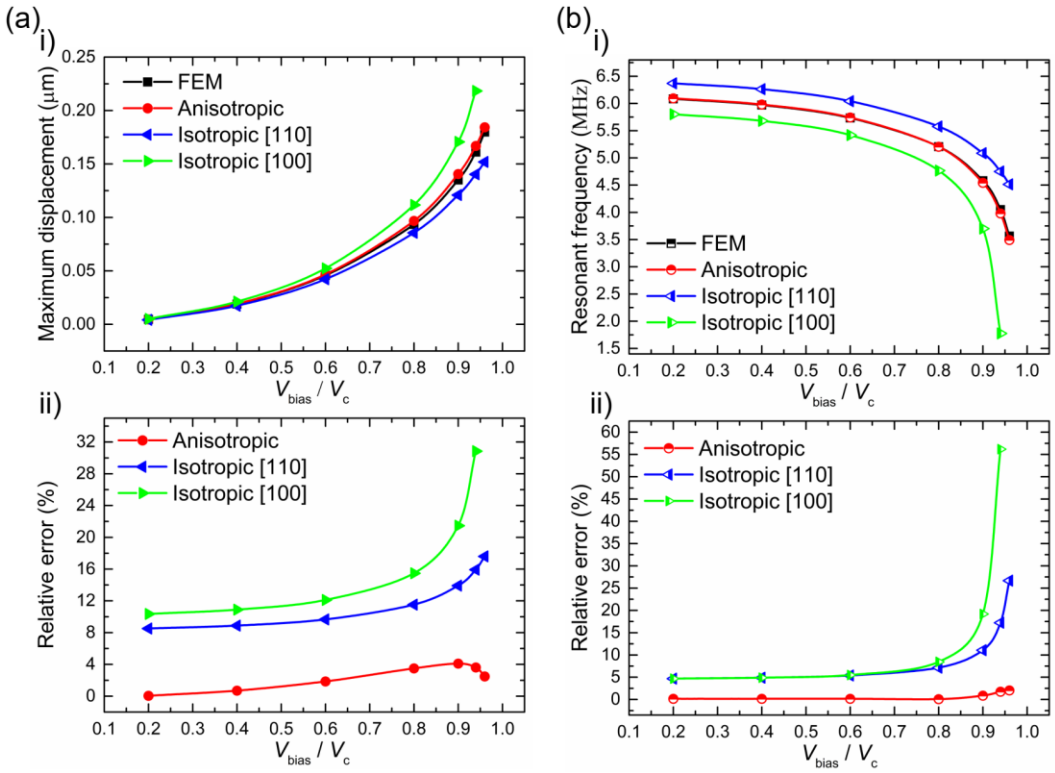

Fig. 2. Comparison of the static deflection and resonant frequency of the (100) silicon-based circular microplate using anisotropic elastic constants with those using the isotropic elastic constants in [100] and [110] directions. (a) Comparison of static defections under different bias voltages; i) static deflections using (16) and FEM simulations; ii) relative difference between the analytical and numerical results. (b) Comparison of resonant frequencies under different bias voltages; i) the first-order resonant frequencies using (32) and FEM simulations; ii) relative difference between the analytical and numerical solutions.

Substituting βR into (30) and setting N to be zero, the first-order resonant frequencies of CMUTs with layered circular anisotropic microplates under electrostatic force and hydrostatic pressure can be given as:

$$f = \frac{10.21}{2\pi R^2}\sqrt{\frac{D'}{\rho_e h}}\sqrt{1-\frac{\varepsilon_0 V_{bias}^2 B}{10.4334 D' R^6}} \tag{32}$$

Equations (16), (18), (30) and (32) can be also used for the static deflection, collapse voltage and resonant frequency analyses of CMUTs with layered isotropic microplates by setting $D' = D_x = D_k = D_y$.

V. Accuracy and Generality Evaluation of Closed-Form Expressions

To evaluate the accuracy and versatility of our closed-form expressions in the analyses of the static deflection, collapsed voltage and resonant frequency of CMUTs with layered circular anisotropic microplates, we compared their analytical results with the numerical ones from FEM simulations. A full 3D FEM model for a CMUT cell was established using ANSYS 15.0, in which the vibrating microplate and electromechanical fields between the top and bottom electrodes were modeled using SOLID185 and TRANS126 elements, respectively. The microplate was assumed to be a single-layer plate made of (100) silicon, and its Cartesian coordinate system was aligned with the principle material direction of the silicon, [110] (see Table AI in Appendix A for the used elastic constants). The meshing of the microplate along with the numbers of TRANS126 elements was optimized to obtain reliable and accurate results. The multiphysics solver was used, and static and pre-stress mode analyses were conducted to obtain the numerical solutions to the aforementioned mechanical parameters under different bias voltages, residual stresses and pressures. The studied CMUT cell had a circular vibrating microplate of 50 μm in diameter and 1 μm in thickness and a gap distance of 0.5 μm, with no insulation layers between its top and bottom electrodes.

We first studied the effects of the used material properties on the analysis accuracies of static deflection, resonant frequency and collapse voltage. We observed that the analytical solutions using the anisotropic elastic constants had a significant improvement in accuracy compared to those using isotropic elastic constants, i.e. the elastic constants in [100] and [110] directions [45]. As shown in the studied case (Fig. 2a-i and 2b-i), the analytical static deflection and resonant frequency based on the anisotropic elastic constants overlap with the numerical results obtained by FEM simulations within the bais voltage range of 0~96% of collapse voltages, showing a maximum difference of 4.1% and 2.0%, respectively (Fig. 2a-ii and 2b-ii). However, the analytical solutions based on those frequently used isotropic elastic constants deviate significantly from the numerical solutions with the increased bias voltages,

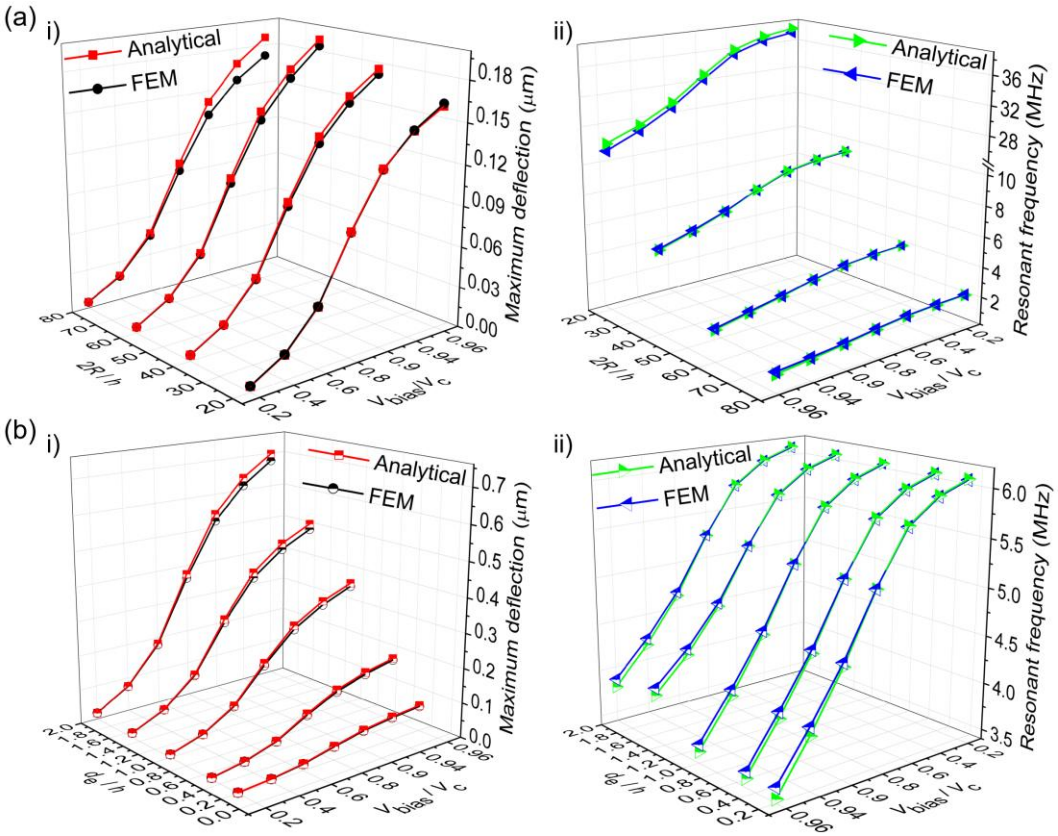

Fig. 3. Comparisons of the analytical results of maximum deflections (center deflection) and resonant frequencies of CMUTs with FEM simulation results under different structure parameters. (a) Deflections and resonant frequencies under different diameter-to-thickness ratios ($2R/h$ = 20, 40, 60 and 80): i) maximum (center) deflection; ii) resonant frequency. (b) Deflections and resonant frequencies under different gap-to-thickness ratios (d_e/h = 0.2, 0.5, 1.0, 1.5 and 2.0): i) maximum (center) deflection; ii) resonant frequency. The analytical results of the deflection and resonant frequency were obtained using (16) and (32), respectively.

showing maximum differences of 30.8% and 56.5% in the static deflection and resonant frequency analyses, respectively (Fig. 2a-ii and 2b-ii). Compared to theories without material anisotropy considered, the closed-form expressions with material anisotropy considered can contribute to at least 7 and 25 times improvement in the analysis accuracies of the deflection and resonant frequency, respectively. Additionally, a comparison of collapse voltages shows that the accuracy of the analytical results considering the material anisotropy is one order of magnitude higher than those neglecting the material anisotropy (Table I). These results demonstrate the necessity of including material anisotropy in the mechanical behavior analysis of CMUTs with anisotropic microplates.

TABLE I
COLLAPSE VOLTAGES OF THE CMUT WITH/WITHOUT THE MATERIAL ANISOTROPY CONSIDERED

Source	Anisotropic (FEM)	Anisotropic (analytical)	Isotropic [110] (analytical)	Isotropic [100] (analytical)
Pull-in voltage (V)	116.0	116.2	121.4	110.7
Relative error	-	0.1%	4.7%	-4.6%

To validate their accuracy and applicability within a wide range of dimension sizes, we conducted a parametric study on the derived closed-form expressions by changing one dimension and keeping the others fixed. We first studied the analysis accuracy of the static deflection, resonant frequency and collapse voltage within the diameter-to-thickness ratio ($2R/h$) range of 20~80 by changing the diameter of the circular microplate. The analytical results of the static deflection and resonant frequency show maximum differences of 4.6% and 4.0%, respectively, from those numerical results across the diameter-to-thickness ratio range of 20~60 and bias voltages of 0~ 96% of collapse voltages, V_c, (Fig. 3a-i and 3a-ii). The maximum differences increase to 8.4% and 10.2% for the static deflection and resonant frequency, respectively, at the $2R/h$ of 80 and 96% V_c. However, the differences decrease rapidly with reduced bias voltages, 7.8% and 3.5% for the static deflection and resonant frequency, respectively, at 90% V_c. This indicates that the $2R/h$ of 80 could be a limit of the applicable dimension range for our closed-form expressions. Besides, the analytical collapse voltages are excellently consistent with the numerical results, showing a maximum difference of 3.0% (Fig. 4a). These results demonstrate that our closed-form expressions can predict the aforementioned mechanical parameters of CMUTs across the wide ranges of diameter-to-thickness ratios ($2R/h$, 20~80) and bias voltages (V_{bias}, 0~96% V_c).

We further studied the accuracy of the closed-form expressions in the analysis of the concerned mechanical parameters under different gap-to-thickness ratios (d_e/h) by changing the gap distance. Excellent agreement between the theoretical analysis and FEM simulations were observed across the gap-to-thickness ratios of 0.2~2. The analytical results of the deflection and resonant frequency show the maximum differences of 4.1% and 2.2% from the numerical results, within almost the whole bias voltage range, up to 96%V_c (Fig. 3b-i and 3b-ii). Additionally, the analytical collapse voltages almost overlap with those numerical results, showing a

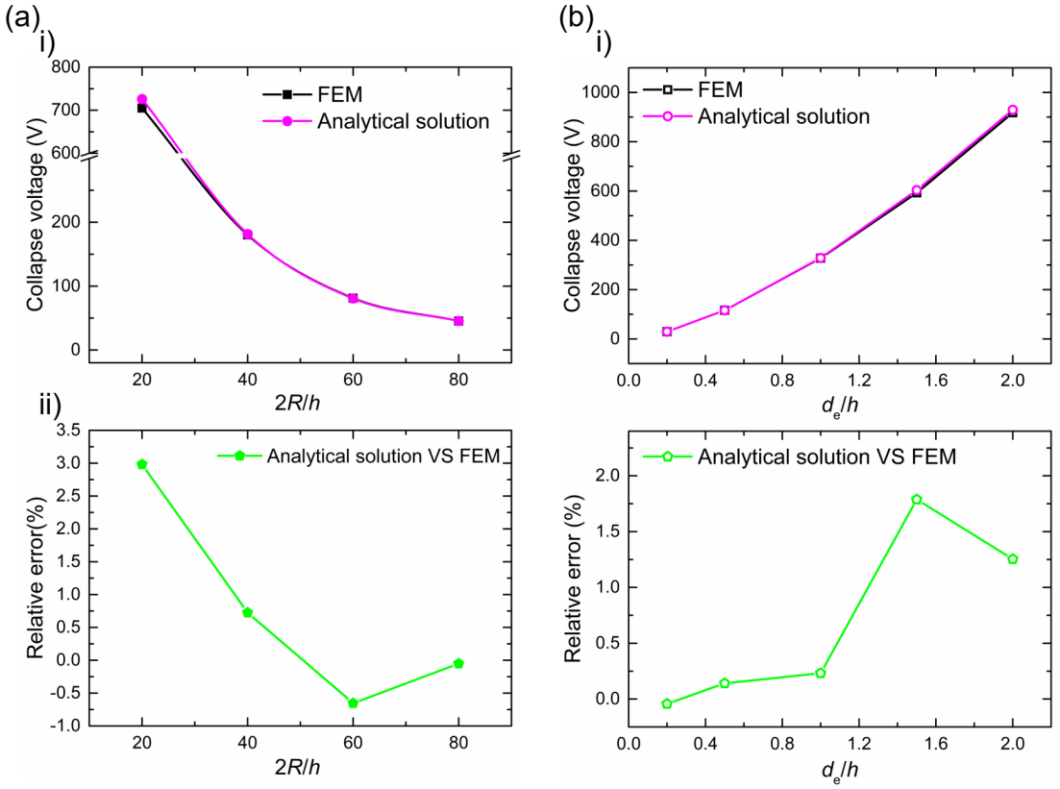

Fig.4. Comparison of collapse voltages between theoretical analysis and FEM simulations. (a) Collapse voltages under different diameter-to-thickness ratios; i) analytical and numerical solutions to collapsed voltages; ii) relative difference analysis. (b) Collapsed voltages under different gap-to-thickness ratios; i) analytical and numerical results of collapse voltages; ii) relative difference analysis.

maximum difference of 1.8% across the dimension range mentioned above (Fig. 4b). These results demonstrate that our closed-form expressions retain high accuracy in analyses of the static deflection, resonant frequency and collapse voltage of CMUTs across a wide gap-to-thickness ratio and almost the whole working voltage ranges.

Subsequently, we investigated the ability of our closed-form expressions to analyze the effects of residual stress and pressure on the mechanical parameters of CMUTs by changing one load and keeping the other two fixed (the applied bias voltage and pressure, or the applied bias voltage and residual stress). We observed that both analytical results of the mechanical parameters under residual stresses and pressures agreed well with those FEM-simulation-based results. For instance, within the studied residual stress range of 0~120 MPa, the analytical results of the collapse voltages, static deflection and resonant frequency agree well with those numerical results, within the differences of 3.4% and 7.5% and 0.2%, respectively (Fig.5a). The analytical deflection shows a higher difference because the residual stress casues middle-plane stretching and harden the stiffness, however, which could be compensated to reduce the difference at high DC voltages because of the enhanced electrostatic-softening effects. Additionally, within the studied pressure range of 0~130 kPa, the analytical results of the aformentioned mechanical parameters also show excellent agreements with numerical results, with the maximum differences of 0.04% and 0.13% in the static deflection and resonant frequency analyses, respectively (Fig.5b). These results indicate that our closed-form expressions can accurately predict the effects of residual stress and pressure on the aforementioned mechanical parameters of CMUTs with circular anisotropic vibrating microplates.

VI. Application of Closed-Form Expressions on CMUTs

In this section, results under more realistic conditions were used to validate our closed-form expressions and highlight their utility in practical applications. We first evaluated the expressions using numerical results based on a boundary condition emulating the reality of the CMUT vibrating microplate, where its lower surface attached to the post was assumed to be fully clamped, while its vertical edges were only constrained in the radial direction (Fig. 6a). This is different from the simplified boundary conditions used in the theoretical analysis and the FEM simulations in Section V where only the movable area of the vibrating plate with a radius of R was considered and its vertical edges were assumed to be fully clamped (Fig. 1b). Comparisons between the analytical results and the FEM-simulation-based results under both fully clamped and more realistic conditions (different post widths[49]) yields two conclusions. 1) The differences of the analytical results from the simulated results under different post widths slightly increases compared to those from the simulated results under fully clamped edges. For instance, the maximum difference increases from 4.1% to 6.2% for deflection analysis (Fig. 6b), and from 2.0% to 9.1% (4.8% under bias voltages of lower than 83%V_c) for resonant frequency analysis under bias voltages lower than 93% of the collapse voltages of the vibrating microplate with the post width considered (Figure. 6c). The difference in the collapse voltage analysis increases from the 0.17% to 4.1% (Fig. 6d). 2) the difference between the

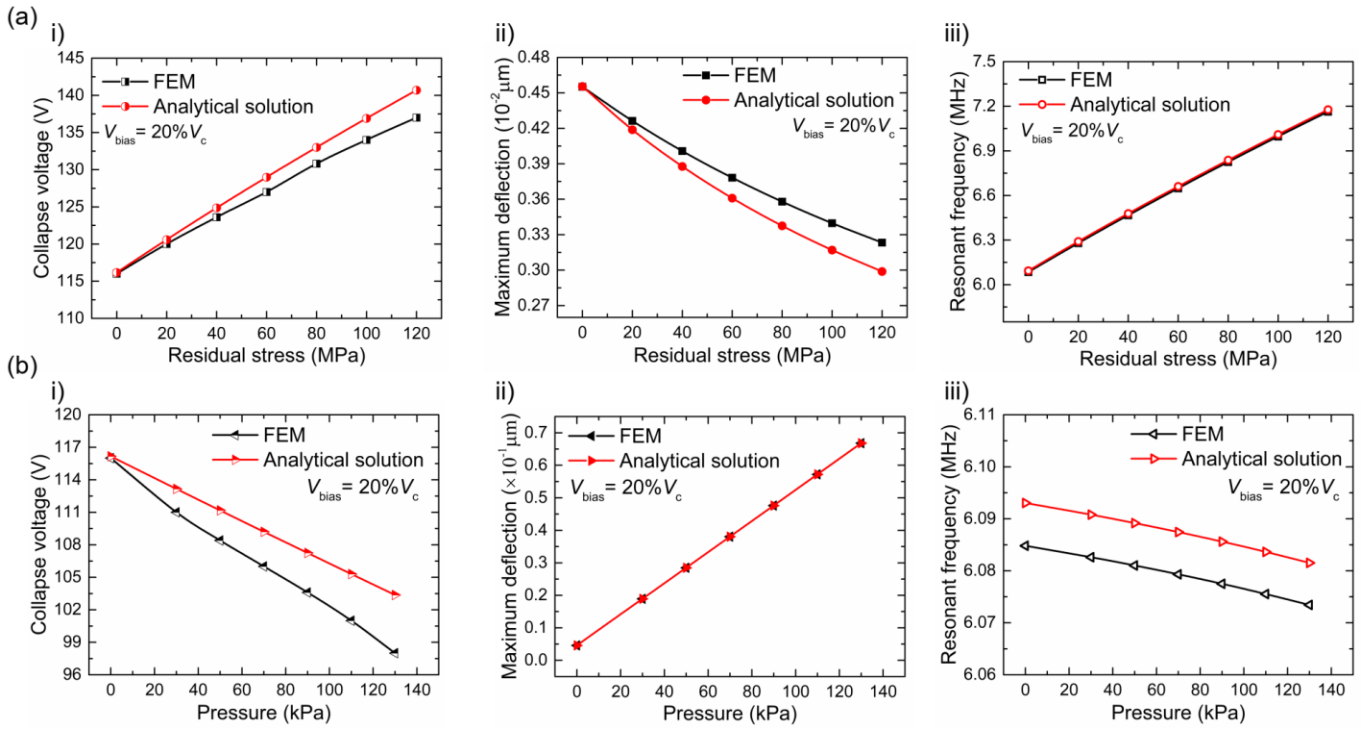

Fig. 5. Comparison of the collapse voltage, static deflection and resonant frequency of CMUT under different residual stresses or pressures with a fixed DC bias voltages of 20%V_c (23.2V). (a) The analytical and numerical results of the collapse voltage, static deflection and resonant frequency under residual stress of 0 to 120 MPa ; i) collapse voltages; ii) static deflection; iii) resonant frequency. (b) The analytical and numerical results of the collapse voltage, static deflection and resonant frequency under pressure of 0 to 130 KPa; i) collapse voltages; ii) static deflection; iii) resonant frequency.

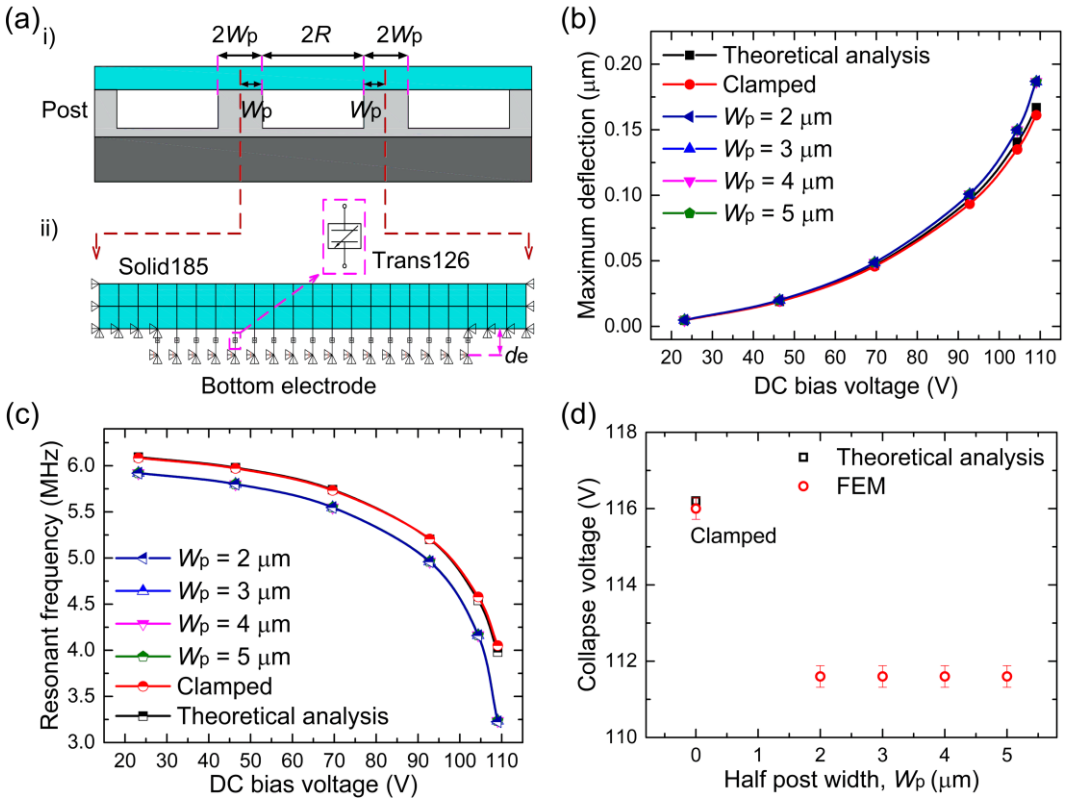

Fig. 6. Effects of practical boundary conditions of CMUTs on the analysis accuracy of closed-form expressions. (a) Schematic of CMUTs and FEM model with the post width considered; i) Structure schematic of multiple CMUT cells with minimum post width, $2W_p$; 2) Cross-sectional view of a 3D FEM model of a CMUT cell extracted from the multiple CMUTs, where the CMUT cell is assumed to have the half post width, W_p (b) Comparison of CMUT deflections considering the post width with that considering fully clamped edges. (c) Comparison of CMUT resonant frequency between the results considering the post width and considered fully clamped edges. (d) Comparison of CMUT collapse voltages under conditions of different post widths and full clamped edges, where the simulated collapse voltages fluctuate within 0.3 V. In the FEM simulations, the basic structure parameters of the CMUT cell were used, and the post widths were chosen as 4, 6, 8 and 10 μm, which were frequently used in CMUTs [49].

analytical results and the numerical results under more realistic boundary conditions are independent of the post width because the numerical results of the deflection, resonant frequency and collapse voltage under different post widths overlap with each other (Fig. 6b-d). Although the closed-form expressions show an increased difference compared with the numerical results under more realistic boundary conditions, their analysis accuracy is still accurate enough for practical applications. Furthermore, the difference estimation under practical boundary conditions enables the closed-form expressions to provide a more reliable prediction for the mechanical parameters of CMUTs, which has been rarely studied in previous theories.

Subsequently, the experimental results of two types of CMUTs chips were employed to further validate the potential of the closed-form expressions . The first type of CMUTs, fabricated by our group [50], has three layers of vibrating microplates composed of a (100) silicon layer, a SiO_2 insulation layer and an aluminum electrode from bottom to top. The layered vibrating microplate has an original gap distance of 0.48 μm with respect to the SiO_2 insulation layer on the silicon substrate (bottom electrode), and an initial deflection of 0.77 μm, which was attributed to the coaction of residual stress and atmospheric pressure (see Table II for the measured structure parameters). Figures 7a-c show comparisons of the experimental results of the deformation shape, static deflection, and resonant frequency of the CMUTs under different bias voltages with the analytical results obtained by our closed-form expressions. The experimental results of the static deflection and collapse voltage were measured using a white-light interference microscope (Talysurf CCI6000, Taylor Hobson Ltd., UK), and the resonant frequency was measured by an impedance analyzer (E4990A, Agilent Technologies, Inc.,

TABLE II
MEASURED STRUCTURE PARAMETERS OF THE FABRICATED CMUTS WITH THE CIRCULAR LAMINATED ANISOTROPIC MICROPLATE

Parameters	value
Radius of the layered plate (R)	59.5 μm
Thickness of silicon layer (h_1)	2.0 μm
Top insulation layer (h_2)	0.20 μm
Aluminum electrode (h_3)	0.41 μm
Bottom insulation layer (h_i)	0.10 μm
Vacuum cavity (d_0)	0.48 μm

TABLE III
MATERIAL PROPERTIES OF THE SiO_2 AND ALUMINUM USED FOR THE MECHANICAL BEHAVIOR ANALYSIS OF CMUTS

Material	Young's modulus (GPa)	Passion's ratio	Density (kg/m^3)	Relative permittivity
SiO_2 (isotropic)	73.1	0.17	2270	3.8
Aluminum (isotropic)	67.7	0.35	2700	-

USA) with a SourceMeter (Keithley 2612A, Tektronix Inc., USA) to supply the DC bias voltage. The residual stress in the three-layer vibrating anisotropic microplate of the CMUTs chips was estimated to be 120 MPa using a 3D FEM model according to the conditions of the initial deflection of 0.77 μm and an atmospheric pressure of 0.1 MPa. The theoretical results of the static deflection, collapse voltages and resonant frequency of CMUTs chips were calculated using (16), (18) and (30) based on the material propeties given in Table AI and Table III.

As shown in Fig. 7a-c, the experimental results of the deformation shape across the diameter, and the static deflection and resonant frequencies under different bias voltages agree well with those theoretical results . The maximum difference between the tested and theoretical resonant frequencies is 11%, which is a little larger than the difference between the theoretical and simulated results demonstrated in the last section. This could be caused by the electrode charging phenomenon in CMUTs, which produces an external voltage superimposed on the applied DC bias voltage and leads to a lower resonant frequency and a larger deflection, as well as larger changes in the two parameters than their expected results [51]. Additionally, another reason for the increased difference is attibuted to the discrepancy of the boundary conditions between the theoretical analysis and reality in CMUTs. Further, we used the closed-form expressions to predict the mechanical parameters of the second type of CMUTs from [45], which has a two-layer vibrating microplate composed of a (100) silicon layer and an aluminum electrode (Table Ⅳ). Fig. 7d shows that the experimental results of the static deflections almost overlap with the analytical results using our closed-form expressions, showing excellent agreement. Besides, the measured collapsed voltage (140 V) of the CMUTs agrees with the theoretical value (143 V) by (18) within the difference of 2.1%. These results demonstrate the practical capability of our closed-form expressions on the mechanical parameter analysis of CMUTs with layered circular anisotropic microplates.

TABLE Ⅳ
STRUCTURE PARAMETERS OF THE CMUTS WITH A TWO-LAYER MICROPLATE FROM [45]

Parameters	Value
Radius of the layered plate (R)	36 μm
Thickness of silicon layer (h_1)	1.8 μm
Thickness of Al electrode (h_2)	0.2 μm
Thickness of insulation layer (h_i)	0.195 μm
Gap distance (d_0)	0.457 μm

VII. DISCUSSION

In the parametric study, we observed that our closed-form expressions based on the CLTP theory have high analysis accuracy even when the deflection increases up to its thickness, which is 5 times larger than the well-known applicable range (20% of the thickness) of the CLTP theory [52]. This could be attributed to that the electrostatic-softening effects induced by the electrostatic force weaken the stress-stiffening effects

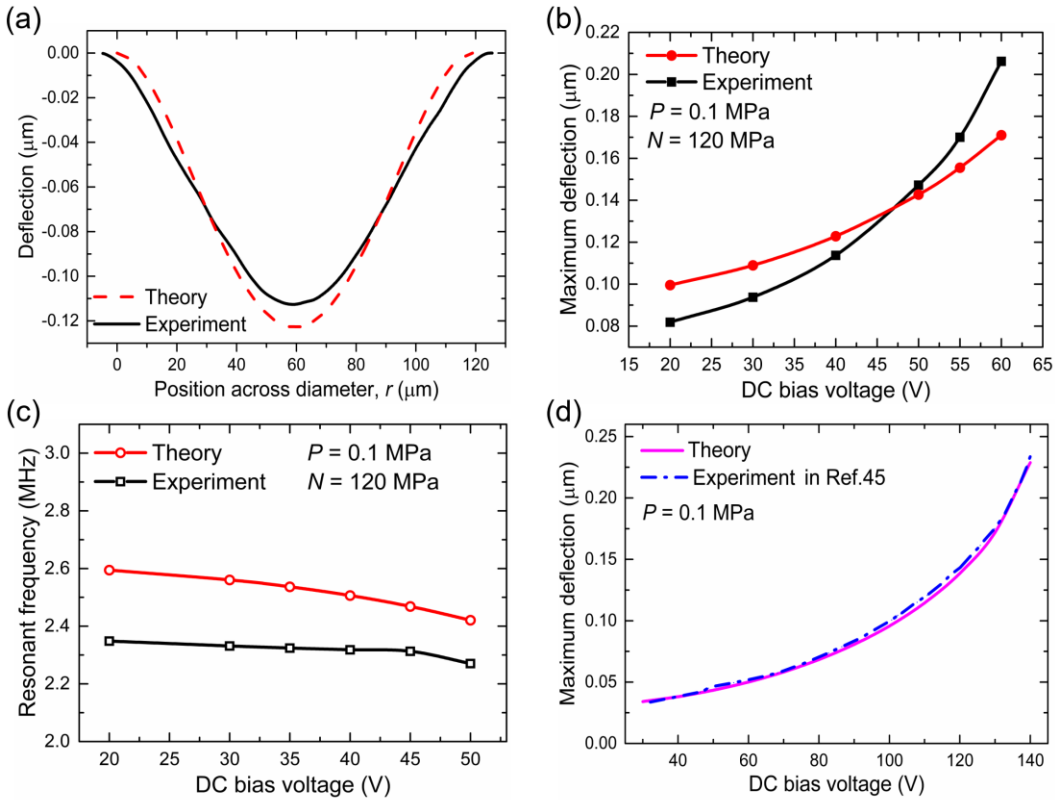

Fig. 7. Validation of our closed-form expressions using experimental data of the fabricated CMUTs chips. (a) The tested and theoretical deformation shapes under a bias voltage of 40 V; (b) a comparison of the deflections of the center point of the vibrating microplate between theoretical and experimental results; (c) the measured and theoretical resonant frequencies under bias voltages from 20 V to 50 V; (d) a comparison of the maximum deflections obtained by our closed-form expressions with the experiment results of CMUTs with two-layer anisotropic microplates from [45].

induced by the middle-plane stretching which generally causes large analysis errors when the deflection increases above the well-known applicable range. To ascertain this point, we further studied the stiffness of electrostatically actuated circular anisotropic microplates with the inclusion and exclusion of the middle-plane stretching. By differentiating the resultant force acting on the microplate, the effective stiffness without taking into account the middle-plane stretching can be given as:

$$D_{\text{eff}} = \frac{\mathrm{d}(F_s - F_e)}{\mathrm{d}w(r)} = \frac{D_0}{(1\text{-}r^2/R^2)^2} - \frac{\varepsilon_0 V_{\text{bias}}^2}{[d_e - w_0(1\text{-}r^2/R^2)^2]^3} \quad (33)$$

where D_0 is the spring-like stiffness of the microplate in the center point, given in (B2) in Appendix B; F_s is the mechanically restoring force per unit area, equal to $D_0 w(r)/[1\text{-}(R\text{-}r)^2]^2$; w_0 is the deflection of the center point under only DC voltage. As shown in (33), the effective stiffness D_{eff} varies over the plate area in the form of the deflection function, $(1\text{-}r^2/R^2)^2$, and decreases with the DC voltage, V_{bias}. To be clear, we focused on the effective stiffness of the center point, which can be derived from (33) by setting r equal to zero as:

$$D_{\text{eff}} = D_0\left(1 - \frac{\varepsilon_0 V_{\text{bias}}^2}{D_0 (d_e - w_0)^3}\right) \quad (34)$$

Further, with a similar method to represent the stress-stiffening effects as in [52], the effective stiffness of the center point with the middle-plane stretching included can be written as:

$$D_{\text{eff}} = D_0\left\{1 + \left(C_s \frac{w_0^2}{h^2} - \frac{\varepsilon_0 V_{\text{bias}}^2}{D_0 (d_e - w_0)^3}\right)\right\} \quad (35)$$

where the term, $C_s w_0^2/h_2$, represents the stress-stiffening effect, and C_s is the coefficient to be determined. Generally, the stress-stiffening effect increases the effective stiffness of microplates with the increased deflection. However, for electrostatically actuated microplates, the stress-stiffening effects can be decreased by the electrostatic-softening effects shown in (35). A parametric study on the effective stiffness based on a circular isotropic microplate shows that the effective stiffness with only the stress-stiffening effect considered increases with the deflection and is larger than the one without the stress-stiffening effect (D_i) considered (Fig.8). However, the effective stiffness considering both the stress-stiffening and electrostatic-softening effects decreases with the increased deflection, and is less than D_i (Fig. 8a). The softened stiffness can contribute to a larger deflection compared with that of the microplate without the action of electrostatic force under the same load. In other words, under the same deflection condition, the middle plane stretching-induced stress of electrostatically actuated microplate is smaller than that of the microplate under common loads such as pressure, resulting in reduced errors. A further study conducted by us shows that the results of deflections (resonant frequency) using FEM simulations with the stress-stiffening effects turned on/off overlap with each other, showing a minimum deviation of 0.45%, even when the deflection increases close to the thickness (Fig. 8b). These indicate that the stress-stiffening effects are negligible and do not cause large errors within the thickness-comparable deflection range for electrostatically actuated microplates. The classical thin plate theory can be used for the analysis of the deflection of electrostatically actuated microplates in an extended range (up to the thickness) without sacrificing the accuracy, revealing the underlying reason for high analysis accuracy of our closed-form expressions.

VIII. Conclusions

In summary, we propose closed-form expressions for the mechanical parameter analysis of CMUTs with layered circular anisotropic microplates subjected to residual stress and hydrostatic pressure by combining the CLTP theory, Galerkin method, a partial expansion approach to approximate electrostatic force and an energy equivalent method. These closed-form expressions are well validated by a

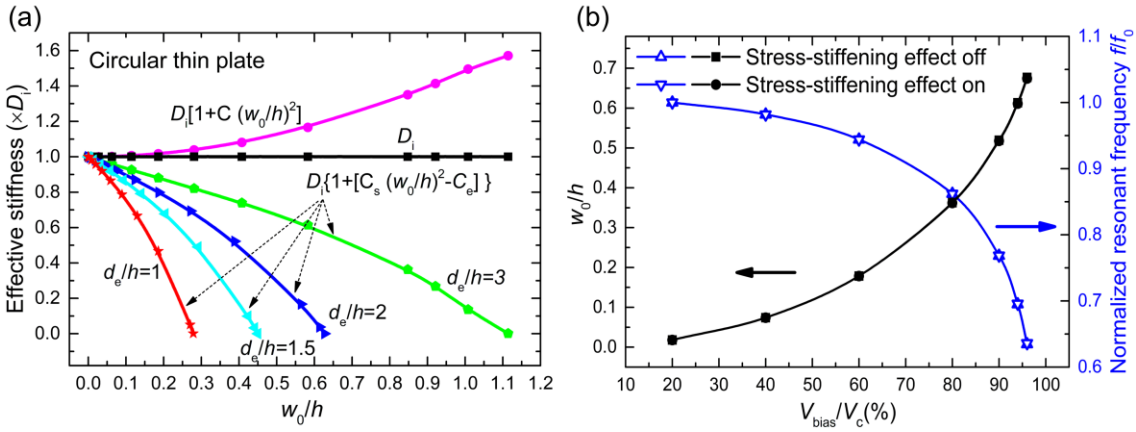

Fig. 8. Effective stiffness of circular vibrating microplates of CMUTs with/without consideration of the effects of middle-plane stretching and the comparison of the static defection (resonant frequency) under the aforementioned conditions.(a) The effective stiffnesses under different deflection-to-thickness ratios. D_i $[1+C_s(w_0/h)^2]$ represents the stiffness with the effects of middle-plane stretching considered; C_s is 0.488 from [52] and D_i is the stiffness of circular isotropic microplate without action of electrostatic force; w_0 is the deflection of the center point of the isotropic microplate which can be derived from (16) by setting both pressure and residual stress to be zero (see (B4) in Appendix B). (b) The results of static deflection and resonant frequency with/without the stress-stiffening effects considered, obtained by FEM simulations using the basic parameters in Section V.

FEM-simulation-based parametric study, and their high accuracy and widespread applicability are demonstrated. Besides, the closed-form expressions can also accurately predict the effects of low range residual stress and pressure on the mechanical parameters of CMUTs. More work need to be done toward analyzing the effects of high residual stress and pressure. Furthermore, we demonstrate the capability of our closed-form expressions in practical applications with fabricated CMUT chips and numerical results based on boundary conditions in reality.

Finally, It's demonstrated that the high accuracy of our closed-form expressions, even when the deflection is up to the thickness, is attributed to that the electrostatic-softening effect dominates the mechanical behavior during that deflection range comparable to the thickness. These closed-form expressions, more efficient and accurate compared with those numerical methods, can be widely used for the design and optimization of CMUTs with arbitrary layers of circular anisotropic microplates. Furthermore, they can also be used to establish closed-form approaches for other performance parameter analysis of CMUTs, such as capacitance, electromechanical coupling coefficients and equivalent circuit models.

APPENDIX

Appendix A:

The stiffnesses, D_{11}, D_{12}, D_{22} and D_{66}, of the laminated anisotropic microplates with n layers can be obtained by:

$$D_{11}=\frac{1}{3}\sum_{k=1}^{n}Q_{11}^{k}(z_k^3-z_{k-1}^3), \tag{A1}$$

$$D_{12}=\frac{1}{3}\sum_{k=1}^{n}Q_{12}^{k}(z_k^3-z_{k-1}^3), \tag{A2}$$

$$D_{22}=\frac{1}{3}\sum_{k=1}^{n}Q_{22}^{k}(z_k^3-z_{k-1}^3), \tag{A3}$$

$$D_{66}=\frac{1}{3}\sum_{k=1}^{n}Q_{66}^{k}(z_k^3-z_{k-1}^3), \tag{A4}$$

where Q_{11}^k, Q_{12}^k, Q_{22}^k and Q_{66}^k are the elastic constants of the kth layer, given in the common coordinate system of the microplate. These elastic constants result from the transformation of the elastic constants in principal material directions where engineering elastic constants are generally tested. The transformation is necessary since the common coordinate system is not always aligned with the crystal coordinate system. As shown in Fig. A1, the axises x^k and y^k define the crystal coordinate system, and the axises x and y define the common coordinate system. The angle θ^k between them is assumed to be positive when the common coordinate system rotates clockwise to the crystal coordinate system. The elastic constants (represented by $\tilde{Q}_{11}^k$, $\tilde{Q}_{12}^k$, $\tilde{Q}_{22}^k$, and $\tilde{Q}_{66}^k$) in the crystal coordinate system can be expressed in engineering elastic constants as:

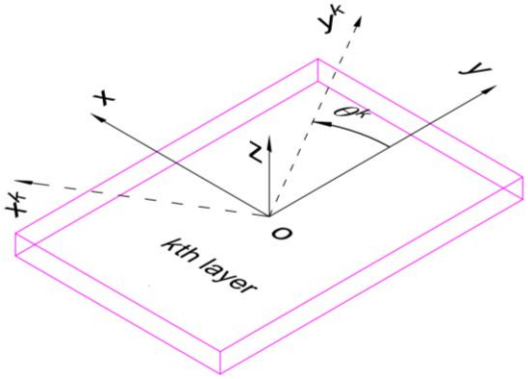

Fig. A1. Schematic of coordinate systems for the transformation of elastic constants

$$\begin{aligned}
Q_{11}^k &= \frac{E_x^k}{1-\mu_{xy}^k\mu_{yx}^k}, \qquad Q_{22}^k=\frac{E_y^k}{1-\mu_{xy}^k\mu_{yx}^k},\\
Q_{12}^k &= \frac{\mu_{xy}^k E_x^k}{1-\mu_{xy}^k\mu_{yx}^k}=\frac{\mu_{yx}^k E_y^k}{1-\mu_{xy}^k\mu_{yx}^k},\\
Q_{66}^k &= G_{xy}^k,
\end{aligned} \tag{A5}$$

The elastic constants in the crystal coordinate system can be transformed into the common coordinate system of the laminated microplate by [42]:

$$\begin{aligned}
Q_{11}^k &= Q_{11}^k\cos^4\theta^k+2(Q_{12}^k+2Q_{66}^k)\sin^2\theta^k\cos^2\theta^k+Q_{22}^k\sin^4\theta^k\\
Q_{12}^k &= (Q_{11}^k+Q_{22}^k-4Q_{66}^k)\sin^2\theta^k\cos^2\theta^k+Q_{12}^k(\sin^4\theta^k+\cos^4\theta^k)\\
Q_{22}^k &= Q_{11}^k\sin^4\theta^k+2(Q_{12}^k+2Q_{66}^k)\sin^2\theta^k\cos^2\theta^k+Q_{22}^k\cos^4\theta^k\\
Q_{66}^k &= (Q_{11}^k+Q_{22}^k-2Q_{12}^k-2Q_{66}^k)\sin^2\theta^k\cos^2\theta^k\\
&\quad +Q_{66}^k(\sin^4\theta^k+\cos^4\theta^k)
\end{aligned} \tag{A6}$$

The elastic constants of (100) silicon in its principal material directions, [110], are given in Table AI.

The equivalent density and thickness of the circular layered anisotropic microplate of CMUTs can be given by (A7) and (A8), respectively.

TABLE AI
ELASTIC CONSTANTS OF (100) SILICON WITH INCLUSION AND EXCLUSION OF ITS MATERIAL ANISOTROPY

Material	Young's Modulus (GPa)	Shear Modulus (GPa)	Passion's ratio	Density (kg/m^3)
Isotropic[100]	130 (E)	E/[2(1+ν)]	0.28 (ν)	2332
Isotropic[110]	169 (E)	E/[2(1+ν)]	0.064 (ν)	2332
	169 (E_x)	50.9 (G_{xy})	0.064 (ν_{xy})	
Anisotropic	169 (E_y)	79.6 (G_{yz})	0.36 (ν_{yz})	2332
	130 (E_z)	79.6 (G_{zx})	0.28 (ν_{zx})	

$$\rho_e=\frac{h_1\rho_1+h_2\rho_2\cdots+h_n\rho_n}{h_1+h_2\cdots+h_n} \tag{A7}$$

$$h=h_1+h_2\cdots+h_n \tag{A8}$$

Appendix B:

The deflection of CMUTs with layered circular anisotropic microplates under only hydrostatic pressure can be derived

from (6) by eliminating time-related terms and setting both electrostatic force F_e and residual stress N equal to zero. Subsequently, substituting the first-order trail function in (10) into the resultant equation, a closed-form expression for the deflection can be obtained as:

$$w = \frac{R^4 P}{64D'}(1-\frac{r^2}{R^2})^2 \tag{B1}$$

As such, the inherent mechanical stiffness of the microplate can be derived by differentiating the pressure to its deflection, which can be obtained as:

$$D(r) = \frac{64D'}{R^4(1-r^2/R^2)^2} = \frac{D_0}{(1-r^2/R^2)^2} \tag{B2}$$

where D_0 is given as:

$$D_0 = 64D'/R^4 \tag{B3}$$

The dimensionless defection of the circular microplate under electrostatic force can be given as:

$$w_0 = d_e\begin{pmatrix} 0.6563 - 0.1126s^2 \\ -0.1126\sqrt{33.9660 - 34.9682s^2 + s^4} \end{pmatrix} \tag{B4}$$

where s is set as:

$$s = V_{\text{bias}} / V_{\text{c}}, \quad V_{\text{c}} = \frac{5.369 d_{\text{e}}^{3/2} D_{\text{i}}^{1/2}}{R^2 \boldsymbol{\varepsilon}_0^{1/2}} \tag{B5}$$

ACKNOWLEDGMENT

The authors would like to thank Dr. Dejiang Lu for his help in English-editing and writing-reviewing. This work has been supported by National Natural Science Foundation of China (51805423, 51890884, 91748207), National Science Foundation for Distinguished Young Scholars (11625208), the Project of Key Industrial Technology Innovation of Suzhou City-Prospective Application Research (SYG201721), the Research Project of State Key Laboratory of Mechanical System and Vibration (MSV201809), Natural Science Basic Research Plan in Shaanxi Province of China (2018JQ5067), the General Financial Grant from China Postdoctoral Science Foundation (2017M623160), the 111 Program (B12016), and the International Postdoctoral Exchange Fellowship Program (20180067).

REFERENCES

[1] W. Y. Choi, Y. S. Kwak, and K. K. Park, "Fingerprint Imaging System Based on Capacitive Micromachined Ultrasonic Transducer by Using Impediography Method Including Direct Touch and Waveguide Methods," *IEEE Trans Ultrason Ferroelectr Freq Control,* vol. 66, no. 2, pp. 402-411, Feb, 2019.

[2] H.-Y. Tang, Y. Lu, X. Jiang *et al.*, "3-D Ultrasonic Fingerprint Sensor-on-a-Chip," *IEEE Journal of Solid-State Circuits,* vol. 51, no. 11, pp. 2522-2533, 2016.

[3] L. Zhao, Y. Zhao, Y. Xia *et al.*, "A Novel CMUT-Based Resonant Biochemical Sensor Using Electrospinning Technology," *IEEE Transactions on Industrial Electronics,* vol. 66, no. 9, pp. 7356-7365, 2019.

[4] A. Singhvi, K. C. Boyle, M. Fallahpour *et al.*, "A Microwave-Induced Thermoacoustic Imaging System With Non-Contact Ultrasound Detection," *IEEE Transactions on Ultrasonics, Ferroelectrics, and Frequency Control,* vol. 66, no. 10, pp. 1587-1599, 2019.

[5] A. Iula, "Ultrasound Systems for Biometric Recognition," *Sensors,* vol. 19, no. 10, 2019.

[6] W. Y. Choi, S. W. Kwon, Y. H. Kim *et al.*, "Single-Shot Near-Field Volumetric Imaging System for Optical Ultrasound and Photoacoustics Using Capacitive Micromachined Ultrasonic Transducer Without Transmission Mode," *IEEE Transactions on Ultrasonics, Ferroelectrics, and Frequency Control,* vol. 67, no. 6, pp. 1151-1158, 2020.

[7] A. Emadi, and D. A. Buchanan, "An Air-Coupled Multiple Moving Membrane Micromachined Ultrasonic Transducer With Inverse Biasing Functionality," *IEEE Transactions on Ultrasonics, Ferroelectrics, and Frequency Control,* vol. 63, no. 8, pp. 1140-1147, 2016.

[8] M. Khan, T. M. Khan, A. S. Tasdelen *et al.*, "Optimization of a Collapsed Mode CMUT Receiver for Maximum Off-Resonance Sensitivity," *Journal of Microelectromechanical Systems,* vol. 27, no. 5, pp. 921-930, 2018.

[9] S. Na, Z. Li, L. L. P. Wong *et al.*, "An Optimization and Comparative Study of Air-Coupled CMUT Cells With Circular and Annular Geometries," *IEEE Transactions on Ultrasonics, Ferroelectrics, and Frequency Control,* vol. 64, no. 11, pp. 1723-1734, 2017.

[10] K. K. Park, O. Oralkan, and B. T. Khuri-Yakub, "A comparison between conventional and collapse-mode capacitive micromachined ultrasonic transducers in 10-MHz 1-D arrays," *IEEE Transactions on Ultrasonics, Ferroelectrics, and Frequency Control,* vol. 60, no. 6, pp. 1245-1255, 2013.

[11] K.-M. Hu, W.-M. Zhang, H. Yan *et al.*, "Nonlinear pull-in instability of suspended graphene-based sensors," *EPL (Europhysics Letters),* vol. 125, no. 2, 2019.

[12] X. Zhang, L. Yu, Q. Guo *et al.*, "Resonance frequency analysis of a dual-frequency capacitive micromechanical ultrasonic transducer for detecting high and low pressures simultaneously with high sensitivity and linearity," *Journal of Physics D: Applied Physics,* vol. 53, no. 3, 2020.

[13] S. P. Mao, X. Rottenberg, V. Rochus *et al.*, "Modal analysis based equivalent circuit model and its verification for a single cMUT cell," *Journal of Micromechanics and Microengineering,* vol. 27, no. 3, 2017.

[14] M. Maadi, and R. J. Zemp, "A Nonlinear Lumped Equivalent Circuit Model for a Single Uncollapsed Square CMUT Cell," *IEEE Transactions on Ultrasonics, Ferroelectrics, and Frequency Control,* vol. 66, no. 8, pp. 1340-1351, 2019.

[15] I. O. Wygant, M. Kupnik, and B. T. Khuri-Yakub, "An Analytical Model for Capacitive Pressure Transducers With Circular Geometry," *Journal of Microelectromechanical Systems,* vol. 27, no. 3, pp. 448-456, 2018.

[16] A. S. Ergun, G. G. Yaralioglu, and B. T. K.-Y. J. J. o. A. Engineering, "Capacitive Micromachined Ultrasonic Transducers: Theory and Technology," vol. 16, no. 2, pp. p.76-84, 2003.

[17] J. Heller, A. Boulme, D. Alquier *et al.*, "Performance Evaluation of CMUT-Based Ultrasonic Transformers for Galvanic Isolation," *IEEE Transactions on Ultrasonics, Ferroelectrics, and Frequency Control,* vol. 65, no. 4, pp. 617-629, 2018.

[18] M. La Mura, N. A. Lamberti, B. L. Mauti *et al.*, "Acoustic reflectivity minimization in Capacitive Micromachined Ultrasonic Transducers (CMUTs)," *Ultrasonics,* vol. 73, pp. 130-139, 2017.

[19] A. Nabian, G. Rezazadeh, M. Haddad-derafshi *et al.*, "Mechanical behavior of a circular micro plate subjected to uniform hydrostatic and non-uniform electrostatic pressure," *Microsystem Technologies,* vol. 14, no. 2, pp. 235-240, 2007.

[20] S. Talebian, G. Rezazadeh, M. Fathalilou *et al.*, "Effect of temperature on pull-in voltage and natural frequency of an electrostatically actuated microplate," *Mechatronics,* vol. 20, no. 6, pp. 666-673, 2010.

[21] S. Ilyas, F. K. Alfosail, and M. I. Younis, "On the Application of the Multiple Scales Method on Electrostatically Actuated Resonators," *Journal of Computational and Nonlinear Dynamics,* vol. 14, no. 4, 2019.

[22] S. Ilyas, F. K. Alfosail, and M. I. Younis, "On the response of MEMS resonators under generic electrostatic loadings: theoretical analysis," *Nonlinear Dynamics*, 2019.

[23] O. Bochobza-Degani, D. Elata, and Y. Nemirovsky, "An efficient DIPIE algorithm for CAD of electrostatically actuated MEMS devices," *Journal of Microelectromechanical Systems,* vol. 11, no. 5, pp. 612-620, 2002.
[24] Y.-G. Wang, W.-H. Lin, X.-M. Li *et al.*, "Bending and vibration of an electrostatically actuated circular microplate in presence of Casimir force," *Applied Mathematical Modelling,* vol. 35, no. 5, pp. 2348-2357, 2011.
[25] A. Jallouli, N. Kacem, F. Najar *et al.*, "Modeling and experimental characterization of squeeze film effects in nonlinear capacitive circular microplates," *Mechanical Systems and Signal Processing,* vol. 127, pp. 68-88, 2019.
[26] R. C. Batra, M. Porfiri, and D. Spinello, "Reduced-order models for microelectromechanical rectangular and circular plates incorporating the Casimir force," *International Journal of Solids and Structures,* vol. 45, no. 11-12, pp. 3558-3583, 2008.
[27] J. Wang, S. H. Pun, P. U. Mak *et al.*, "Improved Analytical Modeling of Membrane Large Deflection With Lateral Force for the Underwater CMUT Based on Von Kármán Equations," *IEEE Sensors Journal,* vol. 16, no. 17, pp. 6633-6640, 2016.
[28] X. Zhao, E. M. Abdel-Rahman, and A. H. Nayfeh, "A reduced-order model for electrically actuated microplates," *Journal of Micromechanics and Microengineering,* vol. 14, no. 7, pp. 900-906, 2004.
[29] D. I. Caruntu, and R. Oyervides, "Frequency response reduced order model of primary resonance of electrostatically actuated MEMS circular plate resonators," *Communications in Nonlinear Science and Numerical Simulation,* vol. 43, pp. 261-270, 2017.
[30] S. Saghir, and M. I. Younis, "An investigation of the static and dynamic behavior of electrically actuated rectangular microplates," *International Journal of Non-Linear Mechanics,* vol. 85, pp. 81-93, 2016.
[31] L. Medina, R. Gilat, and S. Krylov, "Bistability criterion for electrostatically actuated initially curved micro plates," *International Journal of Engineering Science,* vol. 130, pp. 75-92, 2018.
[32] Y. Zhang, and Y.-p. Zhao, "Numerical and analytical study on the pull-in instability of micro-structure under electrostatic loading," *Sensors and Actuators A: Physical,* vol. 127, no. 2, pp. 366-380, 2006.
[33] L.-D. Liao, P. C. P. Chao, C.-W. Huang *et al.*, "dc dynamic and static pull-in predictions and analysis for electrostatically actuated clamped circular micro-plates based on a continuous model," *Journal of Micromechanics and Microengineering,* vol. 20, no. 2, 2010.
[34] P. C. P. Chao, C. W. Chiu, and C. Y. Tsai, "A novel method to predict the pull-in voltage in a closed form for micro-plates actuated by a distributed electrostatic force," *Journal of Micromechanics and Microengineering,* vol. 16, no. 5, pp. 986-998, 2006.
[35] B. Ahmad, and R. Pratap, "Elasto-Electrostatic Analysis of Circular Microplates Used in Capacitive Micromachined Ultrasonic Transducers," *IEEE Sensors Journal,* vol. 10, no. 11, pp. 1767-1773, 2010.
[36] Z. Li, L. Zhao, Z. Jiang *et al.*, "An Improved Method for the Mechanical Behavior Analysis of Electrostatically Actuated Microplates Under Uniform Hydrostatic Pressure," *Journal of Microelectromechanical Systems,* vol. 24, no. 2, pp. 474-485, 2015.
[37] E. V. Thomsen, K. Reck, G. Skands *et al.*, "Silicon as an anisotropic mechanical material: Deflection of thin crystalline plates," *Sensors and Actuators A: Physical,* vol. 220, pp. 347-364, 2014.
[38] M. Engholm, T. Pedersen, and E. V. Thomsen, "Modeling of plates with multiple anisotropic layers and residual stress," *Sensors and Actuators A: Physical,* vol. 240, pp. 70-79, 2016.
[39] W. Zhang, H. Zhang, S. Jin *et al.*, "An Analytical Model for CMUTs with Square Multilayer Membranes Using the Ritz Method," *Micromachines,* vol. 7, no. 4, 2016.
[40] M. Rahman, J. Hernandez, and S. Chowdhury, "An improved analytical method to design CMUTs with square diaphragms," *IEEE Transactions on Ultrasonics, Ferroelectrics, and Frequency Control,* vol. 60, no. 4, pp. 834-845, 2013.
[41] E. J. A. M. R. Carrera, "Thin Plates and Shells: Theory, Analysis, and Applications, authors:E Ventsel, T Krauthammer," vol. 55, no. 4, pp. 1813–1831, 2001.
[42] C. Hwu, *Anisotropic Elastic Plates*, 2010.
[43] M. A. Hopcroft, W. D. Nix, and T. W. Kenny, "What is the Young's Modulus of Silicon?," *Journal of Microelectromechanical Systems,* vol. 19, no. 2, pp. 229-238, 2010.
[44] H. J. Z. J. o. A. M. Altenbach, and M. Z. F. r. A. M. U. Mechanik, "Book Review: J. N. Reddy, Theory and Analysis of Elastic Plates and Shells," vol. 88, no. 10, pp. 827-827, 2008.
[45] M. F. la Cour, T. L. Christiansen, J. A. Jensen *et al.*, "Electrostatic and small-signal analysis of CMUTs with circular and square anisotropic plates," *IEEE Transactions on Ultrasonics, Ferroelectrics, and Frequency Control,* vol. 62, no. 8, pp. 1563-1579, 2015.
[46] Z. Li, L. Zhao, Z. Ye *et al.*, "Resonant frequency analysis on an electrostatically actuated microplate under uniform hydrostatic pressure," *Journal of Physics D: Applied Physics,* vol. 46, no. 19, 2013.
[47] M. Olfatnia, T. Xu, L. S. Ong *et al.*, "Investigation of residual stress and its effects on the vibrational characteristics of piezoelectric-based multilayered microdiaphragms," *Journal of Micromechanics and Microengineering,* vol. 20, no. 1, 2010.
[48] M. S. J. J. o. t. A. S. o. A. Qatu, "Vibrations of Shells and Plates, Third Edition," vol. 117, no. 4, pp. 1683.
[49] S. Wong, M. Kupnik, Z. Xuefeng *et al.*, "Evaluation of wafer bonded CMUTs with rectangular membranes featuring high fill factor," *IEEE Transactions on Ultrasonics, Ferroelectrics and Frequency Control,* vol. 55, no. 9, pp. 2053-2065, 2008.
[50] L. Zhao, J. Li, Z. Li *et al.*, "Fabrication of capacitive micromachined ultrasonic transducers with low-temperature direct wafer-Bonding technology," *Sensors and Actuators A: Physical,* vol. 264, pp. 63-75, 2017.
[51] J. Munir, Q. Ain, and H. J. Lee, "Reliability issue related to dielectric charging in capacitive micromachined ultrasonic transducers: A review," *Microelectronics Reliability,* vol. 92, pp. 155-167, 2019.
[52] Stephen, *Theory of plates and shells*, 1959.

Dr. Zhikang Li currently serves as an assistant professor in school of mechanical engineering, Xi'an Jiaotong University. He received the B.S. degree in Mechanical Manufacturing and Automation from Xidian University in 2010, and the Ph.D. degree in mechanical engineering from Xi'an Jiaotong University in March 2017. From 2014 to 2015, he joined the group of Professor Liwei Lin at UC Berkeley as a jointly cultivated Ph.D. student for one year. From November 2018, he joined the group of Prof. Ali Khademhosseini as an assistant researcher in the Department of Bioengineering at UCLA. His research interests include N/MEMS, capacitive micromachined ultrasonic transducers (CMUTs), piezoelectric micromachined ultrasonic transducers (PMUTs), skin-like electronics and wearable biosensors.

Dr. Libo Zhao received M.S. degree in Instrument Science and Technology in 2003 and Ph.D. degree in Instrument Science and Technology in 2007, both from Institute of Precision Engineering, Xi'an Jiaotong University, Xi'an, China. He is currently working as a professor in Xi'an Jiaotong University. His research interests include micro and

nanofabrication technology, MEMS sensor technology and precision machining technology.

Yihe Zhao was born in Qingdao, China, in 1993. He received the B.S. degree in mechanical engineering from Ocean University of China, Qingdao, China, in 2015. He is currently working towards the Ph.D. degree in mechanical engineering in the Institute of Precision Engineering, School of Mechanical Engineering, Xi'an Jiaotong University, Xi'an, China. His current research interests include micro- and nano-sensors, and integrated circuits technology, especially for biochemical and ultrasonic applications of capacitive micromachined ultrasonic transducers.

Jie Li currently works toward the Ph.D. degree in school of mechanical engineering, Xi'an Jiaotong University, China. He received the M.S. degree in Henan Polytechnic University, China, in 2015. His current research interests include design, fabrication, and characterization of capacitive micromachined ultrasonic transducers (CMUTs) and MEMS-based density/viscosity sensors.

Tingzhong Xu received the B.S. degree in mechanical engineering from Xi'an Jiaotong University, Xi'an, China, in 2013. Currently, he is a PhD student of the joint Ph.D. program between Xi'an Jiaotong University and the University of New South Wales. His research interests include the design, fabrication, and characterization of MEMS sensors, especially the piezoelectric micromachined ultrasonic transducers (PMUTs) for industrial & biomedical applications and ultra-high sensitive pressure sensor for low pressure sensing.

Kai-Ming Hu received the B.S. degree in mechanical engineering from Central South University, Changsha, China, in 2011, and the M.S. degree and the Ph.D. degree in mechanical engineering from Shanghai Jiao Tong University, Shanghai, China, in 2013 and 2017, respectively. From 2015 to 2017, he was a visiting PhD student at School of Mechanical Engineering, University of California, Berkeley. He is the post-doctor at the State Key Laboratory of Mechanical System and Vibration and School of Mechanical Engineering, Shanghai Jiao Tong University. His research interests include surface effect and adsorption-induced surface effect on nonlinear dynamics in MEMS/NEMS.

Zichen Liu was born in Xi'an, China, in 1996. He recevied the B.S. degree in Biomedical engineering from Xi Jiaotong University, China, in 2018. He is currently working towards the M.S. degree in mechanical engineering in the Institute of Precision Engineering, School of Mechanical Engineering, Xi'an Jiaotong University, Xi'an, China. His current research interests include CMUTs appication, especially for industrial application and biomedical appication.

Yang Ping was born in Xianyang, China, in 1986. She received bachelor degree in English Language and Literature in Northwest University in 2009. She is currently the Office Director of the International Joint Laboratory for Micro/Nano Manufacturing and Measurement Technologies, Scientific Research Secretary of Academician, and the Secretary of the Institute of Precision Engineering, Department of Mechanical Engineering, Xi'an Jiaotong University. She involves in the project managements about the research fields of micro-nano fabrication technology, Micro Electro-Mechanical Systems (MEMS) sensor technology, photoelectric testing technology and instrumentation, etc.

Guoxi Luo received the PhD degree in Instrument Science and Technology in 2016 from Chongqing University, Chongqing, China. He is currently working as an associate professor in Xi'an Jiaotong University. His research interests include micro and nanofabrication technology, nano energy harvesting technology, and electrochemistry.

Qijing Lin received the Ph.D. degree in mechanical engineering from Xi'an Jiaotong University, Xi'an, China, in 2015. He is currently a Research Assistant with Xi'an Jiaotong University.
His current research interests include micromanufacturing/nanomanufacturing and intelligent sensing technology.

Dr. Shiming Zhang is a postdoctoral fellow and subgroup leader on devices in Prof. Ali Khademhosseini Lab at University of California, Los Angeles since 2018. He received the B.S. degree (2009) and M.S. degree (2012) from Jilin University, both in Electrical Engineering. In 2017, he obtained the Ph.D. degree in Chemical Engineering (soft electrical devices) from Ecole Polytechnique, University of Montréal (Canada). His research

interests include organic electronics, organic bioelectronics, soft and healable devices, and wearable biosensors.

Martin Hartel is currently a PhD. Student in the bioengineering department at UC Los Angeles. In 2018 he received a B.S. in Nanoengineering from UC San Diego where he worked with Dr. Joseph Wang developing wearable sensors. He is currently advised by Dr. Ali Khademhosseini and Dr. Paul Weiss where he works to develop microfluidic electrochemical sensors. His other interests include integrating sensors with microphysiological systems for improved cell models.

Wen-Ming Zhang (M'10) received the B.S. degree in mechanical engineering and the M.S. degree in mechanical design and theories from Southern Yangtze University, Wuxi, China, in 2000 and 2003, respectively, and the Ph.D. degree in mechanical engineering from Shanghai Jiao Tong University, Shanghai, China, in 2006. He is currently a Professor with the State Key Laboratory of Mechanical System and Vibration, School of Mechanical Engineering, Shanghai Jiao Tong University. He has been involved in the dynamics and control for micro/nanoelectromechanical systems (MEMS/NEMS). His current research interests include nonlinear dynamics and chaos control, nonlinear vibration and control, coupled parametrically excited microresonators, and the reliability analysis and assessment for MEMS/NEMS application.

Zhuangde Jiang Ph.D, is a professor of Xi'an Jiaotong University and an academician of Chinese Academy of Engineering. He is currently the director of Institute of Precision Engineering (IPE). He is also the vice director of Chinese Society of Micro-Nano Technology (CSMNT) and the executive director of Chinese Mechanical Engineering Society (CMES). He involves in research areas including Micro-Nano fabrication technology, Micro Electro-Mechanical System (MEMS) and sensor technology, ultra-precision machining technology and equipment, photoelectric testing technology and instrumentation, etc.